




Cite this: *Mol. Syst. Des. Eng.*, 2023, 8, 1483

# A luminescent cationic MOF and its polymer composite membrane elicit selective sensing of antibiotics and pesticides in water†

Subhajit Dutta, <sup>‡a</sup> Writakshi Mandal, <sup>‡a</sup> Aamod V. Desai, <sup>a</sup> Sahel Fajal, <sup>a</sup> Gourab K. Dam, <sup>a</sup> Soumya Mukherjee <sup>\*b</sup> and Sujit K. Ghosh <sup>\*ac</sup>

Medicines and pesticides are being used excessively, misused, or abused in recent times, resulting in major environmental contamination and, more specifically, water pollution. Remediation of these anthropogenic wastes in ambient water holds the key to mitigating their bioaccumulation and the subsequent negative health impacts. To address this, here, we present a novel stable cationic metal-organic framework (MOF), [Cd(L)<sub>2</sub>(ClO<sub>4</sub>)<sub>2</sub>·xG]<sub>n</sub> (L = 1,1'-(5'-(4-(1*H*-imidazol-1-yl) phenyl)-[1,1':3',1''-terphenyl]-4,4''-diyl) bis(1*H*-imidazole); G = guest molecules), abbreviated as **iMOF-14C** (iMOF = ionic MOF; C = cationic). Composed of Cd(II), perchlorate and an imidazole ligand L, **iMOF-14C** exhibits selective photoluminescence (PL) quenching towards detecting a specific spectrum of antibiotics and pesticides from the contaminated water. It is also responsive to some nitro-functionalised toxins, viz. nitrofurantoin (NFT), as well as pesticides, including nitrofen (an herbicide) and chloropyrifos (CHPS). **iMOF-14C** presents high selectivity towards these target analytes even in the presence of other interfering antibiotics and pesticides, and it reveals a *turn-off* PL response towards trace levels of NFT and NFZ, with detection limits as low as 100 ppb and 20 ppb, respectively. Furthermore, it detects CHPS and nitrofen at 50 ppb and 250 ppb, respectively, *i.e.*, among all porous solids, **iMOF-14C** stands out with record-high pesticide sensing performance. Upon hybridising **iMOF-14C** with low-cost polymer polyvinylidene fluoride (PVDF), the composite membrane **iMOF-14C@PVDF** overcomes processability issues oft-encountered with MOF powders while also exhibiting efficient sensing of antibiotics in water.

Received 14th January 2023,  
Accepted 24th July 2023

DOI: 10.1039/d3me00008g

rsc.li/molecular-engineering

## Design, System, Application

Limited access to clean drinking water is recognised by the United Nations (SDG6) as one of the global grand challenges. Escalating water pollution is arguably the prime culprit. With spiraling industrialization and urbanization, clean water scarcity is only bound to exacerbate. Several emerging organic microcontaminants, such as, antibiotics and pesticides, are increasingly contributing to this alarming situation, primarily driven by their bioaccumulation caused detriments. Therefore, systematic identification of these highly toxic antibiotics and pesticides is of marked relevance. To break the trade-offs between low sensitivity, poor selectivity, high cost, and recyclability driven by high stability, new bottom-up material design blueprints are primed to be the gamechangers. To this end, luminescent metal-organic frameworks (MOFs), an advanced class of crystalline porous solids emerged as the next generation sensory materials and gained tremendous attention owing to their unique structural advantages such as ease in tunability. In this work, we report the design, synthesis and strategic utilization of a new stable luminescent cationic MOF fabricated with an electron-rich organic backbone. The combined merit of the electron-rich framework backbone and water stability of the MOF was further harnessed towards selectively recognising electron-deficient antibiotics and pesticides in water, in powder form, as well as a MOF-polymer composite.

<sup>a</sup> Department of Chemistry, Indian Institute of Science Education and Research (IISER) Pune, Dr. Homi Bhabha Road, Pashan, Pune 411008, India. E-mail: sghosh@iiserpune.ac.in

<sup>b</sup> Bernal Institute, Department of Chemical Sciences, University of Limerick, Limerick V94 T9PX, Ireland. E-mail: Soumya.Mukherjee@ul.ie

<sup>c</sup> Centre for Water Research, IISER Pune, Pune 411008, India

† Electronic supplementary information (ESI) available. CCDC 2225079. For ESI and crystallographic data in CIF or other electronic format see DOI: <https://doi.org/10.1039/d3me00008g>

‡ These authors contributed equally to this work.

## Introduction

One of the pressing global challenges of current times is water pollution, specifically, the lack of clean water and sanitation.<sup>1,2</sup> According to the United Nations Sustainable Development Goal 6 (SDG6), this is recognised as a basic necessity for all forms of life. A conspicuous increase in global population along with surging urbanization and



energy demand further compounds this problem.<sup>3,4</sup> With the rise in awareness regarding community health and natural water quality, demand for the detection and sequestration of toxic pollutants from sewage water is also gaining importance.<sup>5,6</sup> In this regard, emerging organic contaminants and other anthropogenic contaminants account for a significant share of the pressing problem.<sup>7</sup> In essence, a *water contaminant* is defined under the Safe Drinking Water Act (SDWA) as any foreign chemical, physical, biological or radiological object present in the water.<sup>8</sup> Among the anthropogenic wastes, antibiotics and pesticides are two of the most significant pollutant classes contributing to water pollution at the global scale.<sup>9,10</sup> Antibiotics are a class of drugs with widespread use in treating bacterial infections, animal husbandry, agriculture, and pharmaceutical industries.<sup>11–13</sup> Due to their ability to suppress the growth of many diseases, they are frequently used as medicine in hospitals for both human and veterinary treatments.<sup>14,15</sup> In addition to this, the need for sharp growth in agricultural production also necessitates the usage of antibiotics in the fields for food production, beekeeping, aquaculture, etc.<sup>16,17</sup> However, continuous misuse and abuse of antibiotics can result in excessive levels of antibiotic residues in water bodies, implying a high risk to human health. Antibiotics, as a result, are now considered one of the major anthropogenic pollutants.<sup>18,19</sup> On the other hand, pesticides, a category of emerging organic pollutants, have recently gained the “*matter of concern*” status.<sup>20,21</sup> Modern agriculture heavily depends on the extensive usage of pesticides to elevate production. Pesticides are hazardous to both agricultural pests and to water bodies in which they are drained, culminating in water contamination.<sup>22–24</sup> Prolonged exposure to such hazardous contaminants can adversely affect the nervous system of living organisms, for example, worsening the reproductive and respiratory systems of humans.<sup>25–27</sup> Hence, systematic and routine monitoring of these antibiotics and pesticides in water has evolved as a crucial research issue, enabling us to mitigate the risks associated. To address these issues, effort towards the development and optimization of various analytical techniques have been undertaken in the last few decades. Some of them are Raman spectroscopy (RS), mass spectroscopy (MS), LC with UV detection (LC-UV), liquid chromatography with tandem mass spectrometry (LC-MS), and ion mobility spectroscopy (IMS). All these strategies are typically applied toward sensing organic contaminants.<sup>28–31</sup> However, most of them are handicapped by limitations, such as slow kinetics, low efficiency, high cost, and complex quantification methods, which impede their applicability in more advanced applications. Hence, the development of low-cost, simple, highly sensitive and fast techniques that enable the selective detection of hazardous emerging contaminants has become a research hotspot.<sup>32,33</sup> In this context, fluorometric detection techniques have gained a lot of traction owing to their fast kinetics, ease of handling, low cost, and high sensitivity and selectivity. Moreover, functional porous adsorbents are likely to offer higher selectivity and

sensitivity towards a specific analyte as the pores allow analyte preconcentration.<sup>34–36</sup>

Metal–organic frameworks (MOFs), a relatively new family of crystalline porous materials with potential voids, are self-assembled by the periodic combination of metal ions/clusters and organic linkers.<sup>37</sup> Since their discovery, MOFs have found a variety of potential uses.<sup>38–40</sup> Besides, thanks to their compositional modularity, the luminescence signatures in MOFs can be controlled in a bottom-up manner. Simply put, this is achievable due to the combined contribution of photoluminescence (PL) characteristics of their  $\pi$ -rich (or deficient) organic ligand bridges, functional metal nodes, and adsorbed guest molecules.<sup>34</sup> In this regard, luminescent MOFs (LMOFs) have exhibited their potential in various applications, particularly those addressing environmental concerns.<sup>41–43</sup> A wide spectrum of LMOFs have demonstrated benchmark sensory properties towards detecting small molecules, hazardous gases, heavy metal ions, and toxic organic molecules, often presenting new paradigms of chemosensing.<sup>44–47</sup> Nonetheless, studies on the utilization of ionic LMOFs for selectively detecting organic pollutants are too few and far between.<sup>48–52</sup> The possible explanation for this could be the lack of stable cationic LMOFs, which are still a rarity (<10, source: Web of Science).<sup>48</sup> To overcome this problem, we harnessed a  $\pi$ -electron-rich organic ligand with a highly conjugated aromatic skeleton. As a result, the MOF was highly emissive with major PL contributions from ligand-centred emission. Following the principle of HSAB (hard and soft acids and bases), the neutral and tripodal tris(imidazolate) linker was utilised.<sup>53,54</sup> These factors facilitated metal–ligand coordination to afford a cationic framework featuring high chemical stability, which primarily arises from the complete shielding of the metal centres by the linker scaffolds. Effectively, to form a stable cationic LMOF, we selected the  $d^{10}$  transition metal Cd(II) to coordinate with the highly conjugated tris(imidazolyl) ligand, L, (1,1'-(5'-(4-(1*H*-imidazol-1-yl) phenyl)-[1,1':3',1''-terphenyl]-4,4''-diyl) bis(1*H*-imidazole)). A novel, highly luminescent and hydrolytically stable cationic MOF, namely **iMOF-14C**, was the outcome and was studied herein. To explore its potential as a sensory probe, we strategically combined its a) electron-rich framework and b) water stability towards achieving the selective recognition of electron-deficient antibiotics and pesticides in water. **iMOF-14C** presented a highly sensitive and selective *turn-off* PL detection response towards a particular type of antibiotics and pesticides with ultrafast response times (Scheme 1). The limit of detection (LOD) values were found to be among the lowest reported for MOF-based sensors thus far.

## Experimental details

### Caution

Benzene is a highly toxic and volatile solvent that can exert carcinogenic effects on human beings. Hence, appropriate safety measures were taken prior to its use, and it was





**Scheme 1** The schematic representation of the turn-off fluorescence response of iMOF-14C towards hazardous antibiotics and pesticides.

handled with caution. Cadmium is included in the list of candidate substances of very high concern, according to EU regulation no. 1907/2006 (Registration, Evaluation, Authorisation and restriction of Chemicals, REACH list) and was handled with caution.

### Materials

All the required organic reagents (to prepare the ligand L),  $\text{Cd}(\text{ClO}_4)_2 \cdot x\text{H}_2\text{O}$  and solvents were procured commercially and used without any further purification.

### The synthesis of the linker

The organic ligand 1,1'-(5'-(4-(1*H*-imidazol-1-yl)phenyl)-[1,1':3',1''-terphenyl]-4,4''-diyl) bis(1*H*-imidazole) (L) was synthesised according to a reported protocol (Scheme S1†).<sup>55</sup>

### The synthesis of iMOF-14C

A slow-diffusion crystallization technique was employed to synthesise iMOF-14C (Scheme S2†). The ligand L (10.15 mg, 0.02 mmol) was dissolved in *N,N*-dimethylformamide (DMF) and introduced in a cylinder-shaped glass tube to form the bottom layer. The second layer on top of the linker solution contained 1 mL benzene, which acted as a barrier, slowing down the diffusion of the metal and the ligand solutions. On the very top,  $\text{Cd}(\text{ClO}_4)_2 \cdot x\text{H}_2\text{O}$  (6.22 mg, 0.02 mmol) was introduced in a 1 mL methanolic solution. This three-layered diffusion system was maintained in isolation and was not disturbed. Colourless hexagonal crystals were acquired within 14 days. The single crystals were acquired *via* filtration and washed several times with methanol. Pure iMOF-14C single crystals were obtained (yield ~60%, based on Cd). The iMOF-14C crystals were further solvent-exchanged with MeOH for 48 hours, and all the free solvent molecules were degassed by evacuating the dried crystalline solid at 60°C. The formula of iMOF-14C was calculated by employing the PLATON SQUEEZE function to the crystal structure and found to be  $[\text{Cd}(\text{L})_2(\text{ClO}_4)_2 \cdot x\text{G}]_n$  (G = disordered guest molecules).

### The water stability test

To check the water stability, 50 mg of desolvated iMOF-14C was immersed in 20 mL of deionized (DI) water for 24 h at room temperature. Subsequently, the crystalline compound was accumulated *via* filtration and allowed to dry for further characterisation. In addition, inductively coupled plasma atomic emission spectroscopy (ICP-AES) was performed with the supernatant solution to check for leakage of Cd in the water.

### PL measurements

Fine, activated iMOF-14C powder was employed for the fluorometric sensing studies. 1 mg iMOF-14C powder was dispersed in 2 mL of water, and subsequently, 1 mM stock solutions of various antibiotics (nitrofurazone (NFZ), nitrofurantoin (NFT)) and pesticides like nitrofen (an herbicide) and chloropyrifos (CHPS) (20–300  $\mu\text{L}$ ) in water were individually introduced. The gradual decrease in PL response was observed under constant stirring.

## Results and discussion

### Structural description of iMOF-14C

As stated in the experimental section, iMOF-14C single crystals were acquired *via* slow diffusion of the solutions of ligand (L) and  $\text{Cd}(\text{ClO}_4)_2 \cdot x\text{H}_2\text{O}$  in a ternary solvent combination of DMF, benzene and MeOH at room temperature (Scheme S2†). The single-crystal X-ray diffraction experiments revealed that the two-dimensional (2D) network structure of iMOF-14C crystallized in the *P1* space group (Table S3†). The asymmetric unit of iMOF-14C was found to comprise one  $\text{Cd}(\text{II})$  with 1/2 occupancy, which was further connected to two full ligand units. One  $\text{ClO}_4^-$  anion remained free, occluding the pores, alongside one DMF molecule and other solvent molecules (Fig. 1a, S1 and S2†). Harnessing the five-membered imidazolates as the ligating termini was found to be advantageous to reduced steric crowding around the central  $\text{Cd}(\text{II})$ , which allowed the simultaneous



## Paper

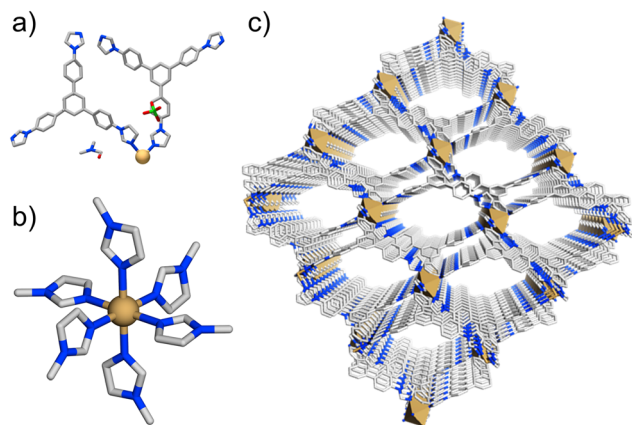


**Fig. 1** The structural representation of **iMOF-14C** illustrating (a) the asymmetric unit and (b) the coordination environment of Cd(II); (c) the view along the *c* axis, showing one-dimensional ultramicroporous (<7 Å) channels that sustain the MOF (colour code: grey – C, blue – N, dark yellow – Cd, red – O, green – Cl; ClO<sub>4</sub><sup>−</sup>, the solvent molecules and hydrogen atoms are omitted for clarity in figures b and c).

coordination with six L units, resulting in the Cd(II)-L octahedral geometry (Fig. 1b, S3†). The average Cd–N bond distance was found to be 2.35 Å. Due to the hydrophobic ligand design of L, **iMOF-14C** exhibited a bi-porous nature, with one small and one large pore contributing to the construction of the framework (Fig. 1c, S4–S8). This characteristic is known to facilitate preferential interactions with incoming guest molecules that exhibit differences in electronic polarisation.<sup>28</sup> **iMOF-14C** was found to have a binodal *kfd* topology with (3,6) connections between the 2D metal–organic sheets, culminating in the intrinsic porosity of the compound. The free ClO<sub>4</sub><sup>−</sup> anions further contributed to counterbalance the residual positive charge in the framework. However, we could not completely locate the free ClO<sub>4</sub><sup>−</sup> anions crystallographically because of crystallographic disorder, but successfully confirmed their presence by Fourier-transform infrared spectroscopy (FTIR), Energy Dispersive X-Ray analysis (EDX) and elemental mapping studies. The PLATON analysis of the **iMOF-14C** structure revealed a guest-accessible volume (excluding anions) of 4591 Å<sup>3</sup>, accounting for *ca.* 58% of the porous nanospace. The structural integrity and bulk phase purity of **iMOF-14C** were confirmed by powder X-ray diffraction (PXRD) analysis, albeit the little variations found in the experimental PXRD pattern. This is attributed to the loss of solvent molecules, a common occurrence that results in the slippage of the 2D layers in layered network structures.<sup>55</sup> Such subnetwork displacement often tends to affect phase purity to varying extents (Fig. S9†).<sup>55</sup> The thermogravimetric analysis of the as-synthesised **iMOF-14C** revealed an initial ~4% weight loss corresponding to the trapped solvent molecules of DMF and water (Fig. S10†). **iMOF-14C** was found to be stable until ~350 °C, which was followed by a significant loss of the organic ligand (*ca.* 400 °C), leading to framework degradation. The FTIR spectra of **iMOF-14C** confirmed the coexistence of all the ligand

characteristic peaks and an additional peak at around ~1100 cm<sup>−1</sup>, indicative of the free ClO<sub>4</sub><sup>−</sup> anions (Fig. S11†). The field-emission scanning electron microscopy (FESEM) images of **iMOF-14C** confirmed the hexagonal morphology of the **iMOF-14C** single crystals, and the EDX spectra revealed the presence of all elements at the expected ratio (Fig. S12–S14†). In addition, the PXRD patterns corroborated well with the water stability of **iMOF-14C**, which can directly be correlated to the hydrophobic shielding offered by Cd(II) flanked by the six independent imidazoles (Fig. S15†). Cadmium concentration was monitored by ICP-AES, revealing the presence of a negligible amount of Cd (0.16 ppm) in the supernatant. This observation also directly supports the hydrolytic stability of **iMOF-14C**.

### Photoluminescence studies

The luminescence quantum yield of **iMOF-14C** was found to be 11.01% (absolute error ± 0.06; relative error ± 5.432 × 10<sup>−4</sup>). Because of its high luminescent nature, we envisioned that **iMOF-14C** can induce selective interactions with guest antibiotic and pesticide molecules, which may lead to variations in PL signatures between **iMOF-14C** and its guest-occluded phases. For **iMOF-14C**, the room-temperature PL spectra were recorded in both the aqueous phase and solid state. The observations alluded to a broad intense single emission spectrum with a peak at 375 nm upon excitation at 330 nm, which can be attributed to either the ligand-centred photoluminescence properties or the emission fingerprint arising from ligand-to-ligand charge transfer (LLCT) (Fig. S16†).<sup>20,21</sup>

### Antibiotic sensing studies

The confluence of the electron-rich backbone, strong luminescence properties and hydrolytic stability of **iMOF-14C** prompted us to explore its potential as a chemosensor in water. To examine its sensory response towards organic micropollutants of different kinds, we conducted photoluminescence spectroscopy experiments with aqueous solutions of several such antibiotics and pesticides (Fig. S17 and S24†). As for antibiotics, we selected nine commonly used antibiotics with different chemical compositions. These included nitrofurantoin (NFT) and nitrofurazone (NFZ) from the class of nitrofurans, sulfaguanidine (SGD) from the class of sulphonamides, ampicillin (AMP) from the class of penicillins, sulfathiazole (STH) from the class of organosulfurs, sulfapyridine (SPD) from the class of sulfonamides, spectinomycin (SPCT), tetracycline (TTC) and kanamycin (KCS). 1 mg of the **iMOF-14C** powder was dispersed in 2 mL water, and the PL emission spectra were recorded subsequently. Thereafter, we introduced a 300 μL aqueous solution (1 mmol) of the selected antibiotics into the mixture individually, and changes in the photophysical properties of **iMOF-14C** were monitored. **iMOF-14C** exhibited 1) rapid PL quenching even under UV-vis light (Fig. 2a and b) and 2) rapid PL quenching towards NFT and







**Fig. 2** Photographs of the emission intensity changes of **iMOF-14C** in water under UV-vis light ( $\lambda = 350$  nm) upon the addition of an (a) aqueous solution of NFT, (b) aqueous solution of NFZ, (c) aqueous solution of CHPS and (d) aqueous solution of nitrofen, each showing rapid quenching of PL emission intensity.

NFZ with incremental addition of the antibiotics in the water medium (Fig. 3a and d and S18 and S19†). On the contrary, it showed insignificant PL quenching towards other selected antibiotics. This observation amply demonstrates the selective fluorescence *turn-off* response of **iMOF-14C** towards the nitrofurant antibiotics, such as NFZ and NFT, which are electron-deficient in nature. Further, the experimental fluorescence data for NFZ and NFT were investigated using the Stern-Volmer (SV) equation, ( $I_0/I = 1 + K_{SV}[Q]$ ), in order to quantify the quenching process, where  $I_0$  and  $I$  stand for the luminescence emission intensity of **iMOF-14C** before and

after the addition of aqueous the antibiotics solution,  $[Q]$  stands for the concentration of the corresponding antibiotics, and  $K_{SV}$  represents the Stern-Volmer Constant (Fig. 3b and e). **iMOF-14C** exhibited a very high  $K_{SV}$  value of  $4.5 \times 10^4 \text{ M}^{-1}$  towards NFT and  $9.9 \times 10^4 \text{ M}^{-1}$  towards NFZ, which stand amongst the best performances reported in the field of porous sensory materials. Furthermore, the LOD values of **iMOF-14C** were estimated to be as low as 100 ppb for NFT and 20 ppb for NFZ (Fig. S20 and S21†). Superior selectivity is another major aspect considered for a sensory material to be upgraded to real-time applicability. To address this aspect, we examined the PL response of **iMOF-14C** towards other selected antibiotics (SGD, AMP, STH, SPD, SPCT, TTC, and KCS) at the same concentration as the nitrofurant antibiotics in water (Fig. S22 and S23†). Interestingly, slight quenching of PL was evident in the case of the other antibiotics. Enthused by these findings, we proceeded further to examine the efficacy of **iMOF-14C** towards the selective recognition of NFT and NFZ in water while the other antibiotics are present (Fig. 3c and f). To execute this experiment, 1 mg of **iMOF-14C** was dispersed in water, and a stock solution of a particular antibiotic was added to it subsequently. After an equilibration time span of 2 minutes, the emission intensities were collected, and further, an aqueous solution of nitrofurant antibiotics was introduced to the solution individually, and the PL spectra were recorded again. Interestingly, we found that the competing antibiotics did not exhibit any substantial alteration in luminescence intensity, but introducing nitrofurant antibiotics resulted in a significant PL quenching

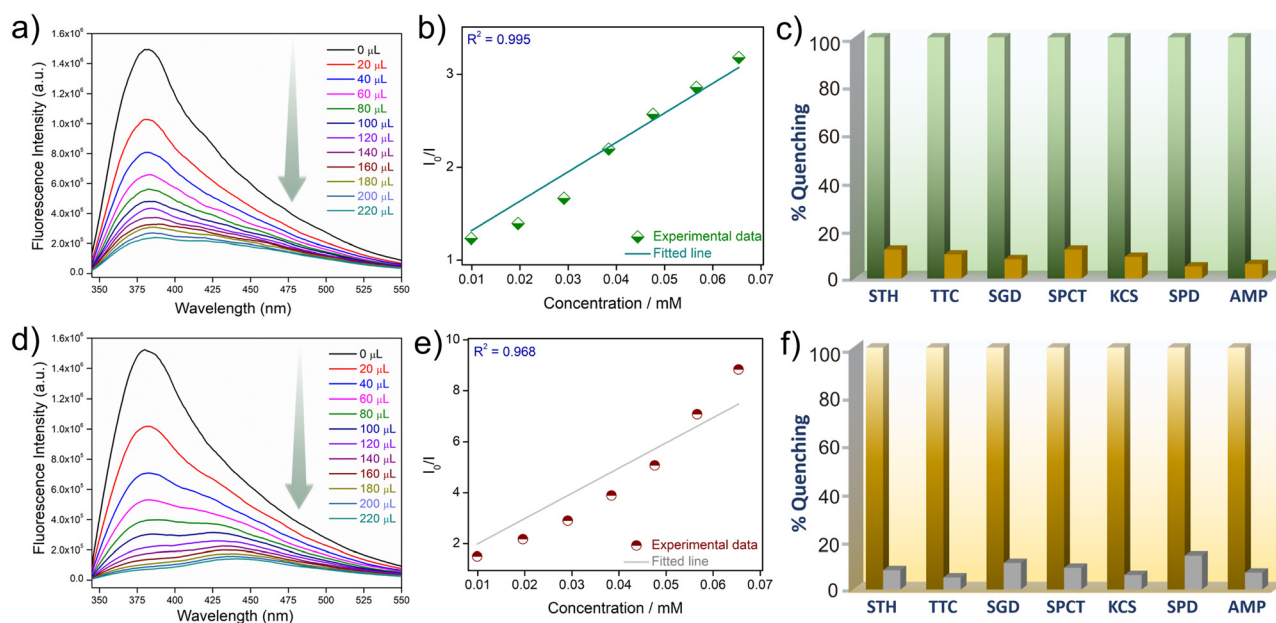


**Fig. 3** (a) The fluorescence *turn-off* response of **iMOF-14C** upon incremental addition of NFT; (b) the Stern-Volmer plot for **iMOF-14C** PL quenched by NFT; (c) the %PL quenching of **iMOF-14C** by the competing analytes alone (brown) and in the presence of their 1:1 binary mixtures with NFT (green); (d) the fluorescence *turn-off* response of **iMOF-14C** upon incremental addition of NFZ; (e) the Stern-Volmer plot for **iMOF-14C** PL quenched by NFZ; (f) the %PL quenching of **iMOF-14C** by the competing analytes alone (brown) and in the presence of their 1:1 binary mixtures with NFZ (green).



of **iMOF-14C** (Fig. 3c and f). The electron-rich nature of the tripodal organic ligand results in the highly electron-rich pore **iMOF-14C** surface, which predominantly interacts with the electron-deficient guest molecules. Considering all the observations, **iMOF-14C** functions as a selective sensor towards nitrofurant antibiotics, and it is arguably a general trend it exhibits towards electron-deficient micropollutants over their electron-rich analogues.

### Pesticide sensing studies

As discussed earlier, apart from toxic antibiotics, aquatic contamination by hazardous pesticides has raised significant ecological concerns. This led us to explore the potential of **iMOF-14C** in recognising hazardous pesticides with good selectivity. For these studies, we selected four different pesticides, namely (2,4-dichloro-1(4-nitrophenoxy)-benzene (nitrofen), chlorpyrifos (CHPS), cypermethrin and fenazaquin (Fig. S24†). Methods similar to antibiotic sensing were followed for the pesticide recognition experiments. **iMOF-14C** showed rapid quenching of fluorescence intensity under the UV-vis light setup, and a luminescence *turn-off* signal with the gradual addition of CHPS and nitrofen (Fig. 2c and d and 4a and d). Further, during the titration experiments, upon the addition of 300  $\mu\text{L}$  (1 mmol) of the aqueous solutions of the four aforementioned pesticides, **iMOF-14C** demonstrated a selective PL quenching behaviour towards CHPS and nitrofen, while the changes in emission response towards the other two pesticides were relatively small (Fig. S25 and S26†). Further, we determined the  $K_{\text{SV}}$

values towards both the pesticides to a) quantify the PL quenching phenomenon and b) establish the relationship between analyte concentration and PL quenching (Fig. 4b and d). **iMOF-14C** registered a very high  $K_{\text{SV}}$  value of  $1.16 \times 10^5 \text{ M}^{-1}$  for CHPS and  $2.01 \times 10^5 \text{ M}^{-1}$  for nitrofen. These values are believed to be among the highest reported among porous materials thus far. In addition, the LOD values for nitrofen and CHPS were estimated by comparing the PL quenching of **iMOF-14C** with the analyte concentration (Fig. 4c and f). The LOD values were found to be as low as 250 ppb and 50 ppb for CHPS and nitrofen, respectively. Such a sensitive detection performance of **iMOF-14C** highlights its potential in the efficient detection of microcontaminants.

To analyse the quenching trend, we compared the emission spectra of **iMOF-14C** with the absorption spectra of the antibiotics and pesticides (Fig. S27 and S28†). In this study, we found significant overlaps between the emission spectra of **iMOF-14C** and the absorption spectra of NFZ and NFT (antibiotics), as well as CHPS and nitrofen (pesticides). These findings are clearly indicative of the energy transfer between the MOF framework and the corresponding analytes, which eventually results in the selective photoluminescence quenching of **iMOF-14C**. Such a significant overlap between the absorption spectra of the targeted antibiotics/pesticides and the emission profile of **iMOF-14C** also highlights the likely contribution of the inner filter effect to PL quenching.

Furthermore, the post-sensing phases of **iMOF-14C** were characterised by confocal fluorescence imaging and FESEM. The FESEM images of the post-recognition stage confirmed that the **iMOF-14C** crystallites retained the morphology (Fig.



**Fig. 4** (a) The fluorescence *turn-off* response of **iMOF-14C** upon incremental addition of CHPS; (b) the Stern-Volmer plot for **iMOF-14C** PL quenched by CHPS; (c) the LOD determination plots for the PL quenching responses of **iMOF-14C** towards CHPS; (d) the fluorescence *turn-off* response of **iMOF-14C** upon incremental addition of nitrofen; (e) the Stern-Volmer plot for **iMOF-14C** quenched by nitrofen; (f) the LOD determination plots correlating with the PL-quenching responses of **iMOF-14C** towards nitrofen.



S29†). We probed the molecule-specific recognition by **iMOF-14C** further *via* confocal fluorescence imaging studies. For this experiment, the effects of NFT and NFZ on the **iMOF-14C** single crystals were monitored under a confocal microscope. The **iMOF-14C** single crystals showed very good luminescence *turn-off* behaviour upon incremental addition of NFT and NFZ (Fig. S30–S32†). Simply put, this study offers direct visual evidence of the PL quenching behaviour of the single crystals of **iMOF-14C**.

### MOF@polymer composite studies

To overcome the practical challenges associated with the processing of powdered MOFs, our current findings

prompted us to develop a standalone **iMOF-14C@PVDF** composite membrane, a prototypical MMM, as a sensory probe for organic micropollutants. Combining **iMOF-14C** with the PVDF polymer (see the ESI† for details) led to the preparation of the **iMOF-14C@PVDF** MMM (Fig. 5a, S33†).<sup>56</sup> The self-standing **iMOF-14C@PVDF** MMM showed strong PL emission behaviour under UV light ( $\lambda = 350$  nm) (Fig. 5b, S33†). Further, to check its antibiotic- and pesticide-sensing performances, we monitored its PL response towards a model antibiotic (NFT) and a pesticide (CHPS). Interestingly, the intense photoluminescence of **iMOF-14C@PVDF** was found to decline rapidly upon the addition of the corresponding antibiotic and pesticide solutions under UV light ( $\lambda = 350$  nm) (Fig. 5b). Further, the solid-state fluorescence emission

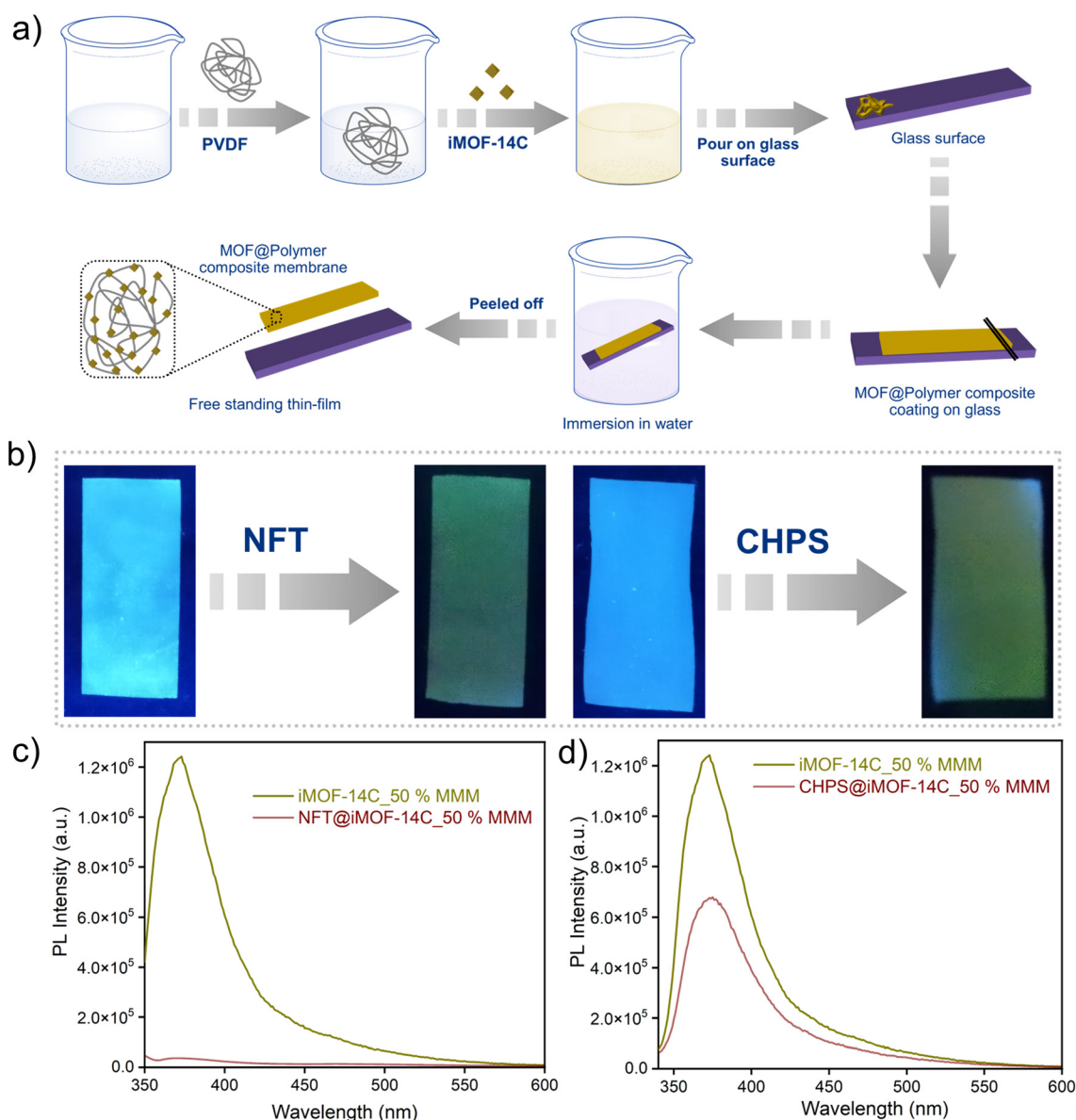


**Fig. 5** a) The schematic illustration of the **iMOF-14C@PVDF** film; PVDF stands for poly (vinylidene fluoride); b) the digital images of self-standing **iMOF-14C@PVDF** MMMs under UV light, and their change in emission properties upon the addition of NFT antibiotic and CHPS pesticide; changes in the fluorescence emission profile of **iMOF-14C@PVDF** upon the addition of c) NFT antibiotic and d) CHPS pesticide.





spectra of iMOF-14C@PVDF were also found to be consistent with the rapid recognition of NFT and CHPS. These observations highlight the yet untapped potential of MMMs, such as iMOF-14C@PVDF, in the real-time aqueous-phase sensing of organic micro-contaminants with enhanced selectivity.

## Conclusion

In summary, a new cationic 2D MOF, namely **iMOF-14C**, was found to demonstrate a rapid and selective fluorescence turn-off recognition response in the water towards hazardous microcontaminants, particularly nitro-functionalised antibiotics and pesticides. Further, **iMOF-14C** possessed excellent selectivity towards the nitrofurantoin antibiotics NFT and NFZ even in the presence of several different types of antibiotics. The quenching constants for NFT and NFZ detection set new benchmarks among porous-solid-based sensors, whereas the corresponding LOD values allude to the real-time application potential of the as-prepared sensing material. In addition, **iMOF-14C** also exhibited very selective and sensitive recognition of specific pesticides, namely CHPS and nitrofen. Overall, **iMOF-14C** was found to selectively detect electron-deficient micropollutants over their electron-rich congeners. This feature was the basis for its translation into **iMOF-14C@PVDF**, a prototypical MOF@polymer composite membrane. In the context of the pressing environmental issue of water pollution by emerging microcontaminants, we believe this work paves a new route towards developing advanced sensory probes designed specifically from MOFs.

## Conflicts of interest

There is no conflict to declare.

## Acknowledgements

S. D., W. M. and A. V. D. thank IISER-Pune for research fellowship. S. F. acknowledges DST-Inspire fellowship (DST/INSPIRE/03/2016/001694). G. K. D. thank CSIR for research fellowship. S. M. acknowledges an SFI-IRC Pathway award (21/PATH-S/9454) from the Science Foundation Ireland. S. K. G. thanks SERB (Project No. CRG/2019/000906) for research funding.

## References

- 1 I. Ali, *Chem. Rev.*, 2012, **112**, 5073–5091.
- 2 S. Rojas and P. Horcajada, *Chem. Rev.*, 2020, **120**, 8378–8415.
- 3 S. B. Grant, J.-D. Saphores, D. L. Feldman, A. J. Hamilton, T. D. Fletcher, P. L. M. Cook, M. Stewardson, B. F. Sanders, L. A. Levin, R. F. Ambrose, A. Deletic, R. Brown, S. C. Jiang, D. Rosso, W. J. Cooper and I. Marusic, *Science*, 2012, **337**, 681–686.
- 4 M. Patel, R. Kumar, K. Kishor, T. Mlsna, C. U. Pittman, Jr. and D. Mohan, *Chem. Rev.*, 2019, **119**, 3510–3673.
- 5 J. Tang, X. Ma, J. Yang, D.-D. Feng and X.-Q. Wang, *Dalton Trans.*, 2020, **49**, 14361–14372.
- 6 S. Dutta, S. Let, S. Sharma, D. Mahato and S. K. Ghosh, *Chem. Rec.*, 2021, **21**, 1666–1680.
- 7 V. Seufert, N. Ramankutty and J. A. Foley, *Nature*, 2012, **485**, 229–232.
- 8 I. Ali, M. Asim and T. A. Khan, *J. Environ. Manage.*, 2012, **113**, 170–183.
- 9 D. J. Lapworth, N. Baran, M. E. Stuart and R. S. Ward, *Environ. Pollut.*, 2012, **163**, 287–303.
- 10 W. Mandal, S. Fajal, P. Samanta, S. Dutta, M. M. Shirolkar, Y. D. More and S. K. Ghosh, *ACS Appl. Polym. Mater.*, 2022, **4**, 8633–8644.
- 11 M. Qiao, G. G. Ying, A. C. Singer and Y. G. Zhu, *Environ. Int.*, 2018, **110**, 160–172.
- 12 E. M. Dias and C. Petit, *J. Mater. Chem. A*, 2015, **3**, 22484–22506.
- 13 W. Yan, Y. Xiao, W. Yan, R. Ding, S. Wang and F. Zhao, *Chem. Eng. J.*, 2019, **358**, 1421–1437.
- 14 D.-W. Sun, L. Huang, H. Pu and J. Ma, *Chem. Soc. Rev.*, 2021, **50**, 1070–1110.
- 15 W.-B. Zhong, R.-X. Li, J. Lv, T. He, M.-M. Xu, B. Wang, L.-H. Xie and J.-R. Li, *Inorg. Chem. Front.*, 2020, **7**, 1161–1171.
- 16 X. Wang, N. Zhuo, C. Fu, Z. Tian, H. Li, J. Zhang, W. Wu, Z. Yang and W. Yang, *Chem. Eng. J.*, 2017, **328**, 816–824.
- 17 N. Xu, Q. Zhang, B. Hou, Q. Cheng and G. Zhang, *Inorg. Chem.*, 2018, **57**, 13330–13340.
- 18 G. Xian, L. Wang, X. Wan, H. Yan, J. Cheng, Y. Chen, J. Lu, Y. Li, D. Li, J. Dou and S. Wang, *Inorg. Chem.*, 2022, **61**, 7238–7250.
- 19 P. Samanta, S. Let, W. Mandal, S. Dutta and S. K. Ghosh, *Inorg. Chem. Front.*, 2020, **7**, 1801–1821.
- 20 M.-L. Xu, Y. Gao, X. X. Han and B. Zhao, *J. Agric. Food Chem.*, 2017, **65**, 6719–6726.
- 21 K. He, Z. Li, L. Wang, Y. Fu, H. Quan, Y. Li, X. Wang, S. Gunasekaran and X. Xu, *ACS Appl. Mater. Interfaces*, 2019, **11**, 26250–26260.
- 22 D. Tilman, K. G. Cassman, P. A. Matson, R. Naylor and S. Polasky, *Nature*, 2002, **418**, 671–677.
- 23 S. T. Narendran, S. N. Meyyanathan and B. Babu, *Food Res. Int.*, 2020, **133**, 109141.
- 24 S. Liu, L. Yuan, X. Yue, Z. Zheng and Z. Tang, *Adv. Powder Technol.*, 2008, **19**, 419–441.
- 25 A. Mojiri, J. L. Zhou, B. Robinson, A. Ohashi, N. Ozaki, T. Kindaichi, H. Farraji and M. Vakili, *Chemosphere*, 2020, **253**, 126646.
- 26 C. L. Tao, B. Chen, X. G. Liu, L. J. Zhou, X. L. Zhu, J. Cao, Z. G. Gu, Z. Zhao, L. Shen and B. Z. Tang, *Chem. Commun.*, 2017, **53**, 9975–9978.
- 27 X. Zhu, B. Li, J. Yang, Y. Li, W. Zhao, J. Shi and J. Gu, *ACS Appl. Mater. Interfaces*, 2015, **7**, 223–231.
- 28 M. Tabrizchi and V. J. Ilbeigi, *J. Hazard. Mater.*, 2010, **176**, 692–696.
- 29 J. Moros, J. A. Lorenzo, P. Lucena, L. M. Tobaria and J. J. Laserna, *Anal. Chem.*, 2010, **82**, 1389.





- 30 K. Håkansson, R. V. Coorey, R. A. Zubarev, V. L. Talrose and P. Håkansson, *J. Mass Spectrom.*, 2000, **35**, 337.
- 31 D. Moreno-González, F. J. Lara, N. Jurgovská, L. Gámiz-Gracia and A. M. García-Campaña, *Anal. Chim. Acta*, 2015, **891**, 321.
- 32 D. Wu, A. C. Sedgwick, T. Gunnlaugsson, E. U. Akkaya, J. Yoon and T. D. James, *Chem. Soc. Rev.*, 2017, **46**, 7105–7123.
- 33 A. Karmakar, P. Samanta, S. Dutta and S. K. Ghosh, *Chem. – Asian J.*, 2019, **14**, 4506–4519.
- 34 H. Wang, W. P. Lustig and J. Li, *Chem. Soc. Rev.*, 2018, **47**, 4729–4756.
- 35 S. Mukherjee, S. Dutta, Y. D. More, S. Fajal and S. K. Ghosh, *Dalton Trans.*, 2021, **50**, 17832–17850.
- 36 S. Mukherjee, D. Sensharma, O. T. Qazvini, S. Dutta, L. K. Macreadie, S. K. Ghosh and R. Babarao, *Coord. Chem. Rev.*, 2021, **437**, 213852.
- 37 H. Li, M. Eddaoudi, M. O’Keeffe and O. M. Yaghi, *Nature*, 1999, **402**, 276–279.
- 38 S. Kitagawa, R. Kitaura and S.-I. Noro, *Angew. Chem., Int. Ed.*, 2004, **43**, 2334–2375.
- 39 S. Mukherjee and S. K. Ghosh, *Nat. Rev. Chem.*, 2021, **5**, 600–601.
- 40 S. Rojas, A. Rodríguez-Diéguez and P. Horcajada, *ACS Appl. Mater. Interfaces*, 2022, **15**, 16983–17007.
- 41 M. D. Allendorf, C. A. Bauer, R. K. Bhakta and R. J. T. Houk, *Chem. Soc. Rev.*, 2009, **38**, 1330–1352.
- 42 W. P. Lustig, S. Mukherjee, N. D. Rudd, A. V. Desai, J. Li and S. K. Ghosh, *Chem. Soc. Rev.*, 2017, **46**, 3242–3285.
- 43 L. E. Kreno, K. Leong, O. K. Farha, M. Allendorf, R. P. V. Duyne and J. T. Hupp, *Chem. Rev.*, 2012, **112**(2), 1105–1125.
- 44 Y. Wang, H. Zhao, X. Li and R. Wang, *J. Mater. Chem. A*, 2016, **4**, 12554–12560.
- 45 I. Tibbetts and G. E. Kostakis, *Molecules*, 2020, **25**, 1291.
- 46 P. R. Lakshmi, P. Nanjan, S. Kannan and S. Shanmugaraju, *Coord. Chem. Rev.*, 2021, **435**, 213793.
- 47 L. Heinke, M. Tu, S. Wannapaiboon, R. A. Fischer and C. Wöll, *Microporous Mesoporous Mater.*, 2015, **216**, 200–215.
- 48 S. Dutta, Y. D. More, S. Fajal, W. Mandal, G. K. Dam and S. K. Ghosh, *Chem. Commun.*, 2022, **58**, 13676–13698.
- 49 H. He, L. Hashemi, M.-L. Hu and A. Morsali, *Coord. Chem. Rev.*, 2018, **376**, 319–347.
- 50 S. Dutta, S. Let, M. M. Shirolkar, A. V. Desai, P. Samanta, S. Fajal, Y. D. More and S. K. Ghosh, *Dalton Trans.*, 2021, **50**, 10133–10141.
- 51 P. Kumar, A. Pournara, K.-H. Kim, V. Bansal, S. Rapti and M. J. Manos, *Coord. Chem. Rev.*, 2017, **86**, 25–74.
- 52 S. Sharma, S. Let, A. V. Desai, S. Dutta, G. Karuppasamy, M. M. Shirolkar, R. Babarao and S. K. Ghosh, *J. Mater. Chem. A*, 2021, **9**, 6499–6507.
- 53 S. Sharma, S. Dutta, G. Dam and S. K. Ghosh, *Chem. – Asian J.*, 2021, **16**, 2569–2587.
- 54 S. Yuan, L. Feng, K. Wang, J. Pang, M. Bosch, C. Lollar, Y. Sun, J. Qin, X. Yang, P. Zhang, Q. Wang, L. Zou, Y. Zhang, L. Zhang, Y. Fang, J. Li and H.-C. Zhou, *Adv. Mater.*, 2018, **30**, 1704303.
- 55 S. Dutta, P. Samanta, B. Joarder, S. Let, D. Mahato, R. Babarao and S. K. Ghosh, *ACS Appl. Mater. Interfaces*, 2020, **12**, 41810–41818.
- 56 M. S. Denny Jr. and S. M. Cohen, *Angew. Chem., Int. Ed.*, 2015, **54**, 9029–9032.

